16

Observations of TIDs over South and Central America

Cesar E. Valladares,[1] Robert Sheehan,[1] and Edgardo E. Pacheco[2]

ABSTRACT

TEC values measured by GPS receivers that belong to the low-latitude ionosphere sensor network (LISN) and several other networks that operate in South and Central America were used to study the characteristics and origin of traveling ionospheric disturbances (TID) in these regions. The TEC perturbations associated with these TIDs show a high degree of spatial coherence over distances > 1000 km allowing us to use measurements from receivers spaced by hundreds of km to calculate the TIDs' travel velocities, propagation direction, and scale size. We first applied the TID analysis to TEC measurements corresponding to 4 July 2011. This processing method is then used to study the characteristics of TIDs for 20 and 21 August 2011, a period when a tropical storm was active in the Caribbean region. A pronounced increase in TID activity was observed in South and Central America at 16 UT on 20 August 2011 lasting until the end of 21 August 2011. The TID velocities show a very variable pattern that depends upon their local time and location. Counter-streaming TIDs were observed over the western part of South America on 21 August 2011. Regional maps of tropospheric temperature brightness, measured by the GOES-12 satellite, are used to identify and follow the development of the tropical storm (TS) Irene and several deep convective plumes. TIDs were observed propagating away from TS Irene. This storm moved into the Caribbean region and intensified earlier on 20 August spawning a train of atmospheric gravity waves (AGW). The small scale size, the velocity less than 150 m/s, and the close location of several TIDs with respect to TS Irene indicate that these TIDs may be the result of primary AGWs that reached the F-region bottomside. These results open the possibility to use TEC values measured by networks of GPS receivers to construct regional, and probably global, maps of TIDs, identify their origin, and study in detail the characteristics of TIDs corresponding to primary and secondary AGWs.

Key Points:
Regional maps of traveling ionospheric disturbances
Primary and secondary gravity waves
Networks of GPS receivers

Key Terms: atmospheric gravity waves, distributed observatory, traveling ionospheric disturbances

16.1. INTRODUCTION

Atmospheric gravity waves (GW) are buoyancy waves that have a dynamic characterized by the interplay between gravity, pressure gradient, and inertial force [*Hocke and Schlegel*, 1996]. Traveling ionospheric disturbances (TID) are the ionospheric response to the passage of GWs [*Hines*, 1960].

[1]*Institute for Scientific Research, Boston College, Newton, Massachusetts, USA*
[2]*Instituto Geofísico del Perú, Jicamarca Radio Observatory, Lima, Lima, Peru*

Ionospheric Space Weather: Longitude and Hemispheric Dependences and Lower Atmosphere Forcing, Geophysical Monograph 220, First Edition. Edited by Timothy Fuller-Rowell, Endawoke Yizengaw, Patricia H. Doherty, and Sunanda Basu.

Gravity waves produce perturbations in the plasma density, ion velocity, and ion and electron temperatures. TIDs are often classified as large scale and medium scale, according to their wave velocity and period. Typical scales size for TIDs (medium and large scales) vary between hundreds and thousands of kms, and periods between 15 min and 3 hr. The terminology of medium-scale TIDs (MSTID) also includes buoyancy waves that have been electrified, following the Perkins instability [*Perkins*, 1973]. They mainly occur at mid-latitude regions where the magnetic field lines are tilted.

Several measuring techniques have been used to study the characteristics and morphology of TIDs. Airglow imagers placed at opposite hemispheres have shown the conjugate characteristics of nighttime MSTIDs in the opposite hemisphere [*Otsuka et al.*, 2004; *Shiokawa, et al.*, 2005, *Martinis et al.*, 2011]. Radio beacon receivers in the VHF band have shown that daytime and nighttime TIDs have different seasonal variations of their occurrence and propagation direction [*Jacobson et al.*, 1995]. Similarly, dense networks of GPS receivers have provided 2D maps of TEC perturbations caused by TIDs [*Saito et al.*, 1998; *Afraimovich et al.*, 2001]. The radio beacon technique [*Mercier*, 1986; *Jacobson, and Erickson*, 1992; *Jacobson, et al.*, 1995] overcomes many limitations of other observation methods, enabling continuous characterization of key TID parameters. Although radio beacon TEC measurements are integrated over the whole altitude range of the ionosphere, the vertical localization of GW-induced TEC fluctuations makes this technique a powerful tool for studying TIDs that propagate through the F-region bottomside. In addition, observations [*Kirkland, and Jacobson*, 1998] and model results [*Vadas*, 2007] have shown that most TIDs do not commonly rise above 400 km. Thus, the bulk of the TEC perturbations become highly localized to the bottomside region.

The modeling study of *Vadas and Liu* [2009] has shown that the dissipation of "primary" GWs can create localized thermospheric body forces able to excite "secondary" large-scale TIDs with a wavelength close to 2100 km, velocity near 500 m/s, and a period of ~80 min. *Vadas and Crowley* [2010] have presented evidence that multiple convective plumes can create thermospheric body forces containing smaller scales due to constructive and destructive wave interference. Such body forces are able to excite secondary GWs with smaller horizontal scale sizes. These authors were able to relate TID observations conducted with the TIDDBIT sounder [*Crowley and Rodrigues*, 2012] and the development of a tropical storm and several convective plumes that appeared in the Caribbean region. *Vadas and Crowley* [2010] found TIDs having large phase speeds, which were too large to have originated from convective overshoot. Therefore, they postulated that these waves were originated in the upper mesosphere and thermosphere.

In the radio beacon technique, also known as radio interferometry, phase differences measured at the various stations can be used to determine TID velocity, propagation azimuth, and amplitude. Recently, this radio-interferometry technique has been adapted for use with GPS satellites [*Afraimovich et al.*, 1998, 2000, 2003]. This new innovation makes it possible to utilize inexpensive, easily deployed GPS receivers to study gravity waves at a wide variety of locations. The large number of GPS satellites in orbit makes it possible for a single receiver to continuously monitor the bottomside region at multiple ionospheric locations simultaneously. Recently, *Valladares and Hei* [2012] used a GPS-radio interferometer to measure the phase velocity and propagation direction of gravity waves that were propagating near Huancayo (12.042°S, 75.321°W) in Peru. The phase velocity and direction of propagation were extracted by using two algorithms: the Statistical Angle of Arrival and Doppler Method for GPS interferometry (SADM-GPS) and the cross-correlation method (CCM). Both methods agreed that on 20 July 2008 between 22 and 24 UT, several TIDs moved across the small array of GPS receivers with a velocity near 130 m/s, were directed northward and had wavelengths close to 450 km. The CCM method was later applied to TEC values collected by other GPS receivers that were operating hundreds of kilometers away from Huancayo providing phase velocities close to 150 m/s [*Valladares and Chau*, 2012]. This new method offers the possibility to exploit measurements from adjacent GPS receivers to study the characteristics of TID within a much larger region.

The main goal of this chapter is to describe the results of a method that produces regional maps of TEC perturbations associated with TIDs within the South and Central America regions and to relate these observations to maps of tropospheric brightness temperature measured by the GOES-12 satellite. GOES-12 satellite images are used to pinpoint the locations of deep convective plumes across South and Central America and the existence of tropical storms that move throughout the Caribbean region on 20 and 21 August 2011. The chapter is organized in the following order: In Section 16.2, we introduce the general characteristics of the cross-correlation analysis that was applied in a regional context to extract the characteristics (e.g., occurrence, velocity, scale size) of the TIDs of 4 July 2011. Results of the regional analysis of the TEC observations recorded by hundreds of GPS receivers on 20 and 21 August 2011 are presented in Section 16.3. The association of TIDs with tropical storms and convective plumes imaged with the GOES-12 satellite are presented in Section 16.4. The discussion section and the main conclusions of the chapter are presented in Sections 16.5 and 16.6.

16.2. ANALYSIS OF TEC OBSERVATIONS FOR 4 JULY 2011

The low-latitude Ionospheric Sensor Network (LISN) is a distributed observatory designed to monitor and specify the condition of the ionosphere over South America in a regional context. LISN provides near real-time observables

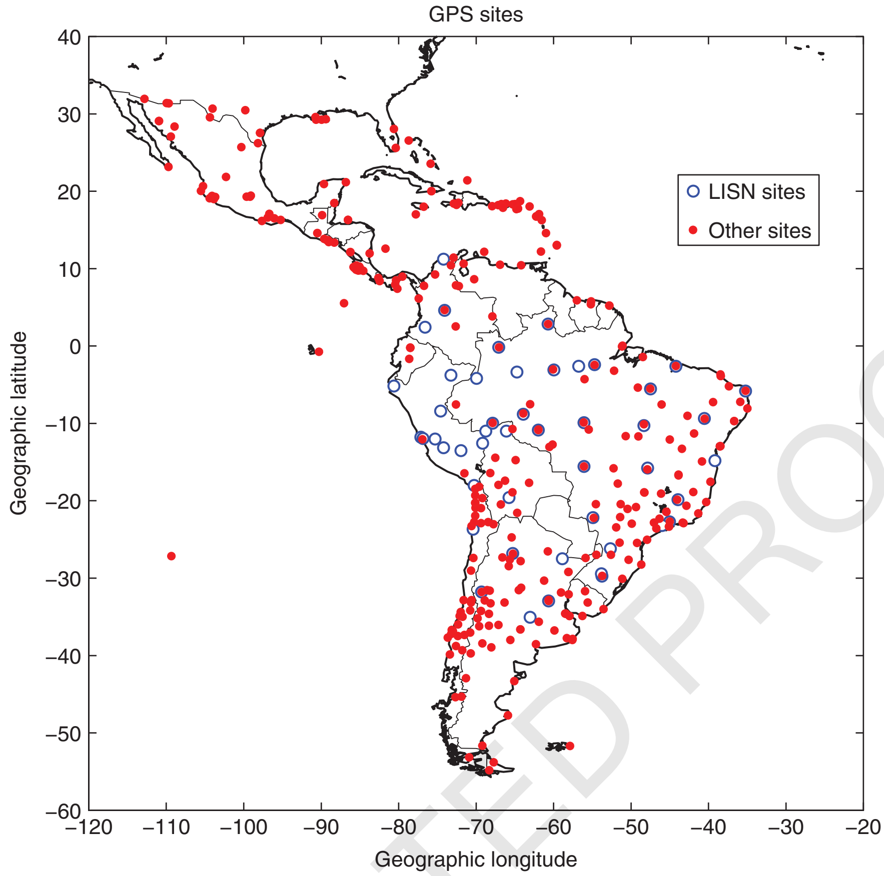

Figure 16.1 Locations of GPS receiver stations installed by the LISN project (blue) and several other networks (red) in South and Central America and the Caribbean region.

(nowcast) from 47 dual-frequency GPS receivers [*Valladares and Chau*, 2012]. Figure 16.1 shows the locations of the LISN GPS receivers (blue circles) together with a much larger number of GPSs (red dots) that belong to several networks currently operating in South and Central America and the Caribbean region. In 2011, a total of 324 GPS receivers operated in South and Central America for ionospheric, plate tectonic, and seismology research, studies of river-land interactions, tropospheric weather, and land surveying. As part of the LISN project, we are processing the RINEX files corresponding to all of these GPS receivers stored in the LISN server. These files are stored in the LISN website for display and dissemination. This section presents the results of an investigation of the regional characteristics of TIDs that were observed on 4 July 2011.

16.2.1. Regional Maps of TEC Perturbations

The TEC perturbations (TECP) of Figure 16.2 were obtained using all the GPS receivers that operated in South and Central America on 4 July 2011. The TECP traces are plotted in red, centered along the satellite subionospheric intersection (short black segments). Note that most of the GPSs did not record any TEC perturbation or their peak values were below the threshold level (0.4 TEC units) leaving blank areas in all three frames. The algorithm to detect TECP removes the 24 hr solar-produced daily TEC variability and excludes other perturbations not directly associated with TIDs (e.g., plasma bubbles). The first step of our TID identification algorithm consists of estimating the background TEC values by fitting a fourth-order polynomial to every 3 hr segment of TEC values and then subtracts these values from the measured TEC. The second step excludes TEC depletions originated by equatorial plasma bubbles or midlatitude depletions by comparing the magnitude of the positive and negative excursions of TEC perturbations. As depletions only produce TEC decreases and TIDs create both positive and negative variations, a positive-to-negative perturbation ratio between 0.66 and 1.3 was selected for a valid detection of a TID. The third step consists of a wavelet-type analysis using quasi-sinusoidal functions to extract the amplitude and scale size of the TIDs. The last step involves a low-pass filter to eliminate noise signals containing periods smaller than 5 min. In addition, the automatic identification of TIDs is restricted to wave periods between 90 and 15 min. On many occasions, we observed TEC perturbations with two or more spectral peaks produced by the transit of

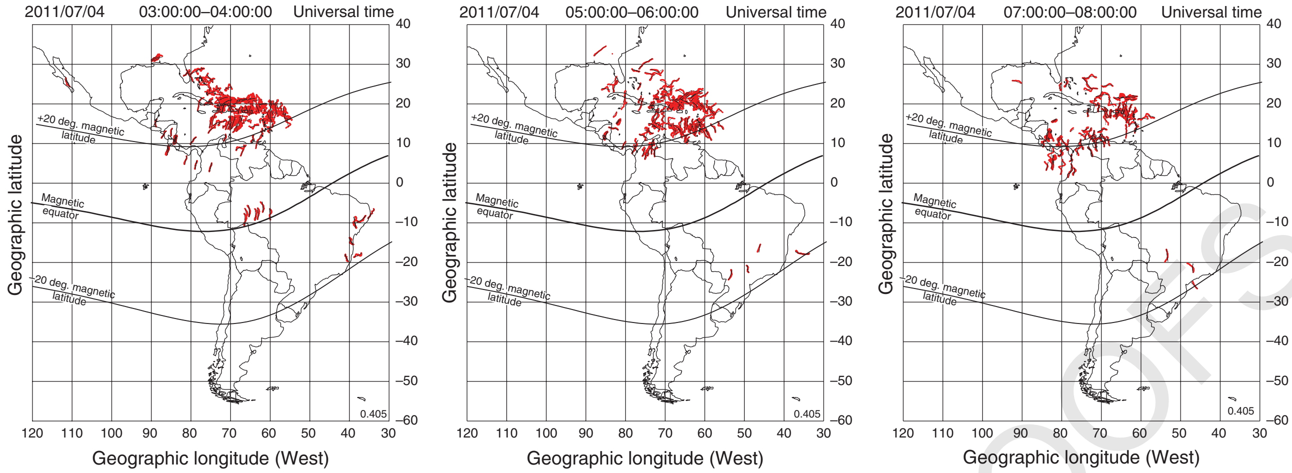

Figure 16.2 TEC perturbation (TECP) values measured with all the GPS receivers that operated on 4 July 2011 during three time intervals (03–04, 05–06 and 07–08 UT). The red traces correspond to the TECP values after subtracting the daily variability. The thin black traces indicate the locations of the ionospheric piercing points at 350 km altitude.

multiple TIDs propagating simultaneously through the same volume. During these cases, we band-pass filtered the dTEC perturbation and only considered the TID that contained the largest amplitude.

Figure 16.2 shows the hour-to-hour variability of the TIDs corresponding to 4 July 2011 observed in South and Central America between 03 and 08 UT and detected automatically using the software described above. This figure depicts TEC perturbations at the latitude and longitude of the subionospheric intersection for each GPS satellite pass and for each station that reported a valid TID detection. The left frame shows TIDs placed mainly at the center of the Caribbean region. Two hours later (center frame), TIDs have expanded southward covering a larger area and populating the northern boundary of South America. The right frame of Figure 16.2 indicates that the TIDs have propagated southward toward lower latitudes; they are sparse and are likely in a decay process. TIDs decayed completely after 08 UT, not only in the Caribbean and Central America region, but also in the South America continent. This behavior of intense TIDs in the Caribbean and Central America regions near midnight and the early hours of the day is quite typical during the June solstice season.

16.2.2. Cross-Correlation Analysis Applied to Regional Network of GPS Receivers

To derive the motion of the TIDs across a continent-size region (regional context), we divide the receivers of Figure 16.1 into small clusters of receivers, varying in number between 3 and 18 GPSs. Only the receivers that have simultaneously observed TIDs with similar amplitudes and periodicities are considered part of the cluster. The TIDs' drift velocity is then calculated employing the software presented by *Valladares and Hei* [2012], in which dTEC values measured by three adjacent receivers are cross-correlated between them to derive the phase drift velocity. Consequently, each cluster is further subdivided in several subgroups of three adjacent receivers and analyzed independently. One receiver acts as the reference point and its location defines the center of the coordinate system. TECP values of this receiver are correlated with the values corresponding to the other two receivers, providing the time offset along two different directions that do not need to be perpendicular. Both time offsets and equations (16.1) and (16.2) are used to resolve the magnitude of the phase velocity ($V_h[t]$) and the propagation angle of the TID ($\acute{a}[t]$).

$$\acute{a}(t)=arctan\left(\left(Y_A T_{B-C}-Y_C T_{B-A}\right)/\left(X_C T_{B-A}-X_A T_{B-C}\right)\right) \tag{16.1}$$

$$V_h(t)=\left(Y_C cos\left(\acute{a}(t)\right)+X_C sin\left(\acute{a}(t)\right)\right)/T_{B-C} + w_x(t)\sin\acute{a}(t)+w_y(t)\cos\acute{a}(t) \tag{16.2}$$

Where T_{B-A} and T_{B-C} are the time delays between the TECP traces. The symbols X_A, Y_A, X_C, and Y_C refer to Cartesian distances between the satellite-receiver pierce points for the reference receiver and the pierce points for both additional receivers (named A and C). The satellite velocity is removed by subtracting the component of the motion of the pierce points ($w_x(t)$ and $w_y(t)$) in the propagation direction of the TIDs. The receiver placed further southwest is commonly designated as the reference receiver (also called B).

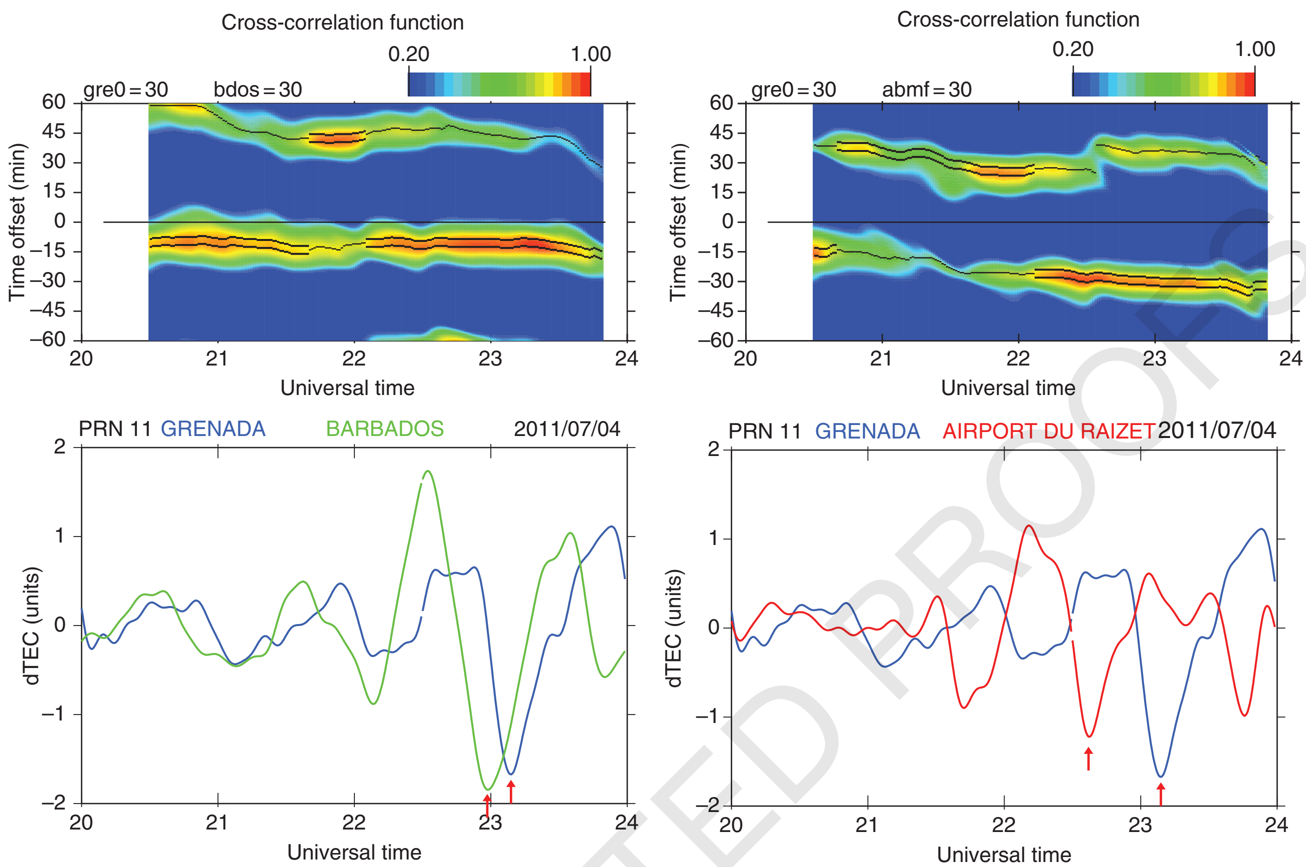

Figure 16.3 Cross-correlation functions (top panels) and TECP curves (lower frames) for GPS satellite 11. The left frames show the CCFs for TECP signals from Grenada and Barbados. The right panels correspond to Grenada and Airport du Raizet. The cross-correlation functions are plotted using a color scale that varies between 0.2 and 1.0. The double black line that crosses near the middle in the top-left frame corresponds to the correlation maximum and it is considered to be the time delay (T_{B-A} or T_{B-C}).

The lower panels of Figure 16.3 show dTEC values from three GPS receivers placed in the Caribbean region. These receivers detected a train of TIDs on 4 July 2011 that lasted for 4 hr. Note that the blue trace, corresponding to Grenada, acts as receiver B and it is displayed in both panels. The dTEC increases after 22 UT attaining peak-to-peak values near 4 TECu. It is also evident that a second TID with much shorter periodicity (10–20 min) and smaller amplitude is superimposed on the near 60 min period of the primary TID. To extract the velocity information of both TIDs (primary and secondary), it is necessary to use a cross-spectrum analysis [*Crowley and Rodrigues*, 2012]. However, we opted for filtering and then analyzing only the period (~60 min) that contains the largest amplitude. All three traces (blue, green, and red) show a high degree of similarity that is reflected in the high correlation factor (~1) displayed in the upper panels. Only positive values of the correlation factor, between 0.2 and 1.0 are color coded in the top panels. The correlation time series show two prominent peaks that are produced by the periodic nature of the dTEC signal associated with a quasi-periodic train of TIDs. However, the time of the first large negative peak of the TID, indicated by the red arrows, is used to discern the correct delay between the dTEC traces. It is evident that a large minimum was observed at Barbados (green trace) just before 23 UT. This was observed at Grenada (blue) a few minutes after 23 UT. A larger delay between the minimum peaks is seen in the right lower panel where the first large minimum at Airport du Raizet (red) occurs at 2240 UT and ~30 min ahead of minimum at Grenada. In summary, this simple analysis helps us to conclude that the TID passed first through Airport du Raizet (abmf), then Barbados (bdos), and at the end through Grenada (gre0). Due to the locations of these three receivers, as seen in the top frame of Figure 16.4, it is concluded that the TIDs' velocity was close to southward.

Figure 16.4 displays a map of the geographic locations of the three GPS receivers (top panel) and the magnitude

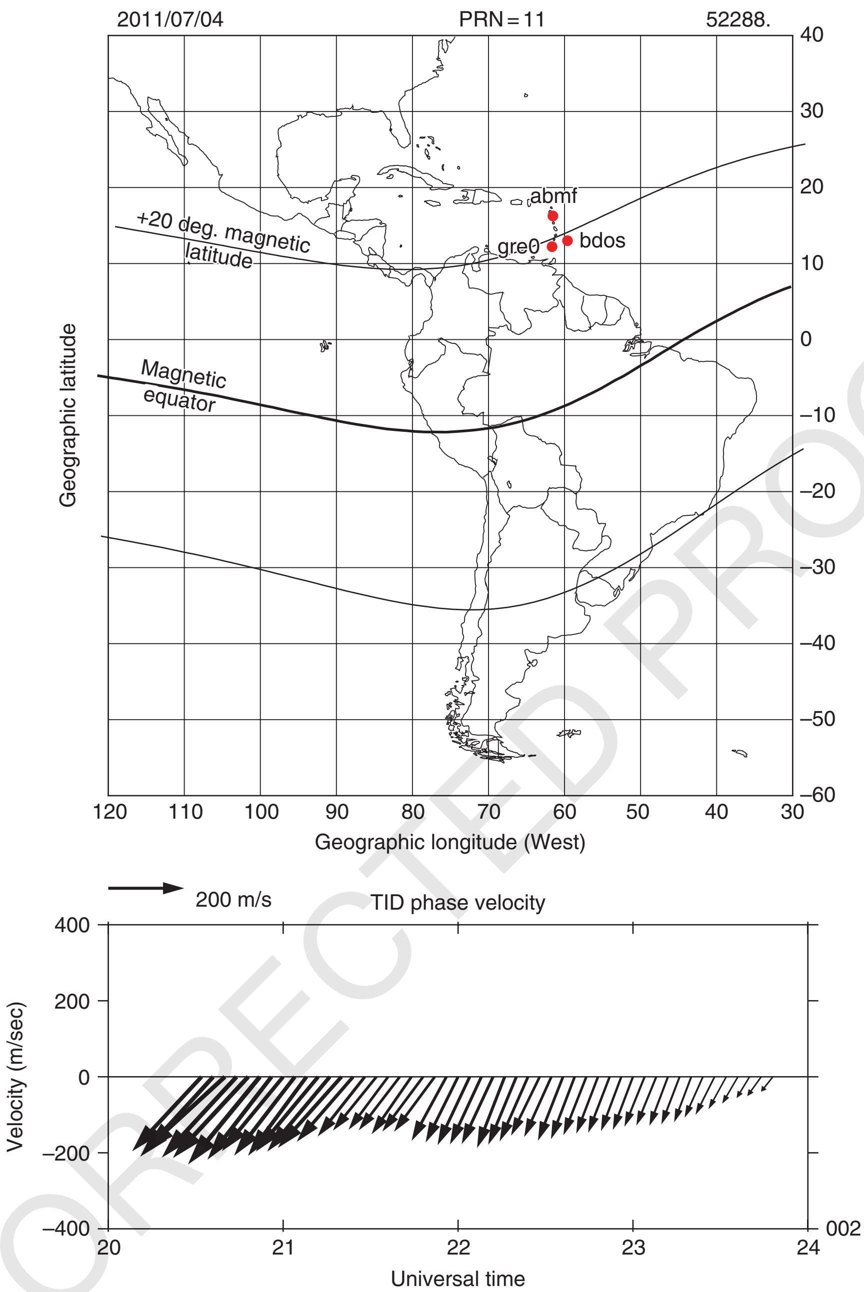

Figure 16.4 The top panel shows the locations of the three stations used in the velocity analysis: Grenada, Barbados, and Airport du Raizet. The lower panel shows the phase velocities of the TIDs calculated using the CCM method and TEC perturbation from all three stations for 4 July 2011.

and direction of the phase velocity derived between 20 and 24 UT (lower panel). The velocity is directed southwest and the magnitude decreases from 250 m/s near 20 UT until it reaches 50 m/s at 24 UT. The more refined and precise calculation of the TID velocity corroborates the intuitive motion of the dTEC perturbation described earlier.

16.3. ANALYSIS OF TEC OBSERVATIONS FOR 20–21 AUGUST 2011

This section describes the analysis of the TIDs that were observed on 20 and 21 August 2011 across South and Central America and the Caribbean region. First, we divided the receivers in clusters of adjacent GPSs that observed TIDs with similar characteristics and during equal time intervals. Then, each cluster was analyzed independently providing a time series of the TIDs' velocity. Finally, all these time series were arranged in time and space to build regional maps of TIDs' velocity over South and Central America. These results allow us to relate regional maps of the occurrence, location, and velocity of the TIDs over the continent and regional maps of tropospheric deep convective cells observed by the GOES-12 satellite. The goal of this section is to relate the dynamics of the TIDs observed on 20–21 August 2011 to the existence of a tropical storm in the Caribbean region and deep convective cells that originated within the central and southern parts of South America.

16.3.1. Regional Maps of TIDs Occurrence for 20–21 August 2011

The regional maps of Figure 16.5 show TEC perturbations associated with the TIDs that developed over South and Central America on 20 and 21 August 2011. Each frame corresponds to a 4 hr interval in which we have plotted all the TIDs detected by the GPS receivers presented in Figure 16.1. The four frames in the top row of Figure 16.5 indicate an absence of TIDs between 00 and 16 UT on 20 August 2011. After this period, TIDs' population increases across the South American continent in a sector limited between −10° and −20° geographic latitude. The following frame, corresponding to the period 20–24 UT, displays dTEC perturbations persisting in South America, across the same latitudinal sector observed 4 hr earlier. This frame also shows TIDs extending between the Caribbean Sea and the eastern part of Central America. These newly developed TIDs remain active until 08 UT on the following day. The South American TIDs decay before the start of day 21 August 2011. However, they reappear after 15 UT on 21 August 2011. In summary, it was observed that on these two days, TIDs developed over South America at latitudes slightly south of the magnetic equator between 16 and 24 UT. In fact, during the following 10 days, TIDs occur very systematically and almost every day between 16 and 24 UT. In Central America, the Caribbean region, and the northern part of South America, TIDs occur at different time epochs and extend through different areas.

16.3.2. Analysis of TIDs Using a Cluster of GPS Receivers

Figure 16.6 displays dTEC perturbations associated with a train of TIDs that were detected by one cluster of 11 GPS receivers between 19 and 24 UT on 20 August 2011. These receivers are located in northern Colombia as shown in the small panel placed in the upper right side. The dTEC values were derived using signals from the GPS satellite PRN = 17. The station's four-letter name, the latitude, and the longitude are indicated in the right margin. Note also that the amplitude of the dTEC is printed at the middle right side and it is equal to 5 TEC units. From top to bottom, the stations are organized following their geographic latitude, starting at the top with the station placed farther north, Santa Marta (lsam), and ending with Bogota (lbo_). These two stations belong to the LISN network. This display arrangement helps us to discern the propagation direction of the TID. We select a conspicuous feature within the dTEC traces, like the largest minimum or maximum, and determine how this feature time shifts at different sites. Red arrows indicate the time when the largest minimum occurs for each of the 11 traces of Figure 16.6. As this feature appears at earlier times at sites that are placed farther south, it is concluded that the TIDs observed on 20 August 2011 in northern Colombia are propagating northward. We also calculate the average period of the TIDs equal to 63 min and the spectral width 44 min. We also indicate that some of the stations present rapid dTEC fluctuations, as seen at Dorada (dora) and Aguachica (agua) at 22 UT. This effect is likely produced by the transit of additional TIDs containing shorter spatial scales.

Figure 16.7 shows the velocity analysis for three stations (Corozal, Cucuta, and Maracaibo) that are part of the cluster of GPS receivers presented in Figure 16.6. To avoid contamination produced by TIDs that have periods different than 63 min and are transiting across the stations with different velocities and scale sizes, we apply a band-pass filter to the dTEC traces and filtered out these unwanted TIDs. The middle frames display the dTEC traces after they have been filtered using a band-pass filter centered at 63 min (0.2 mHz). The top panels display the cross-correlation functions (CCF) in which two peaks separated by ~60 min are evident produced by the periodicity of the TIDs. To determine the peak associated with the true motion of the TIDs, we use the information provided by Figure 16.6 in which it was realized that the TIDs were moving northward. Note that a negative (positive) offset is an indication that Corozal's TEC perturbation lags (leads) Cucuta's. As Corozal is located north of Cucuta and south of Maracaibo, to calculate the TIDs' velocity we considered the CCF peak with a negative delay for the first pair of stations (Corozal and Cucuta) and the positive delay for the second pair (Corozal and Maracaibo). Similar analysis was performed for every set of three different receivers of the cluster of GPSs depicted in Figure 16.6.

The velocity of the train of TIDs is shown in the lower panel of Figure 16.7. This velocity is equal to 250 m/s and directed northward at 20 UT, and becomes northwest-

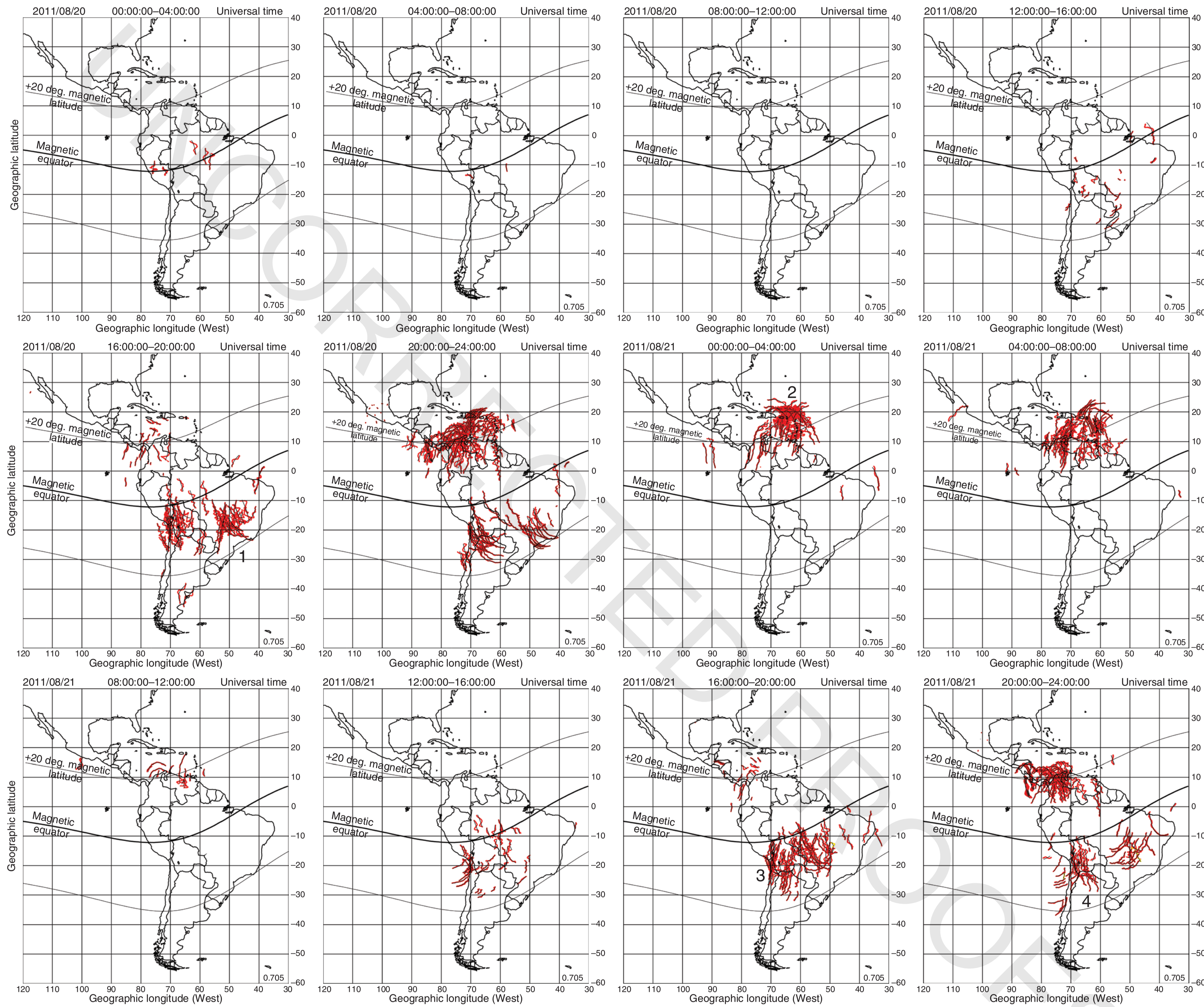

Figure 16.5 Same as Figure 16.2, but for TIDs measured on 20 and 21 August 2011. Each panel displays the amount of TIDs observed during a 4 hr segment. Each red segment indicates the location of a TID detected by our analysis package. Large spaces without red traces are the result of the absence of TIDs in those regions.

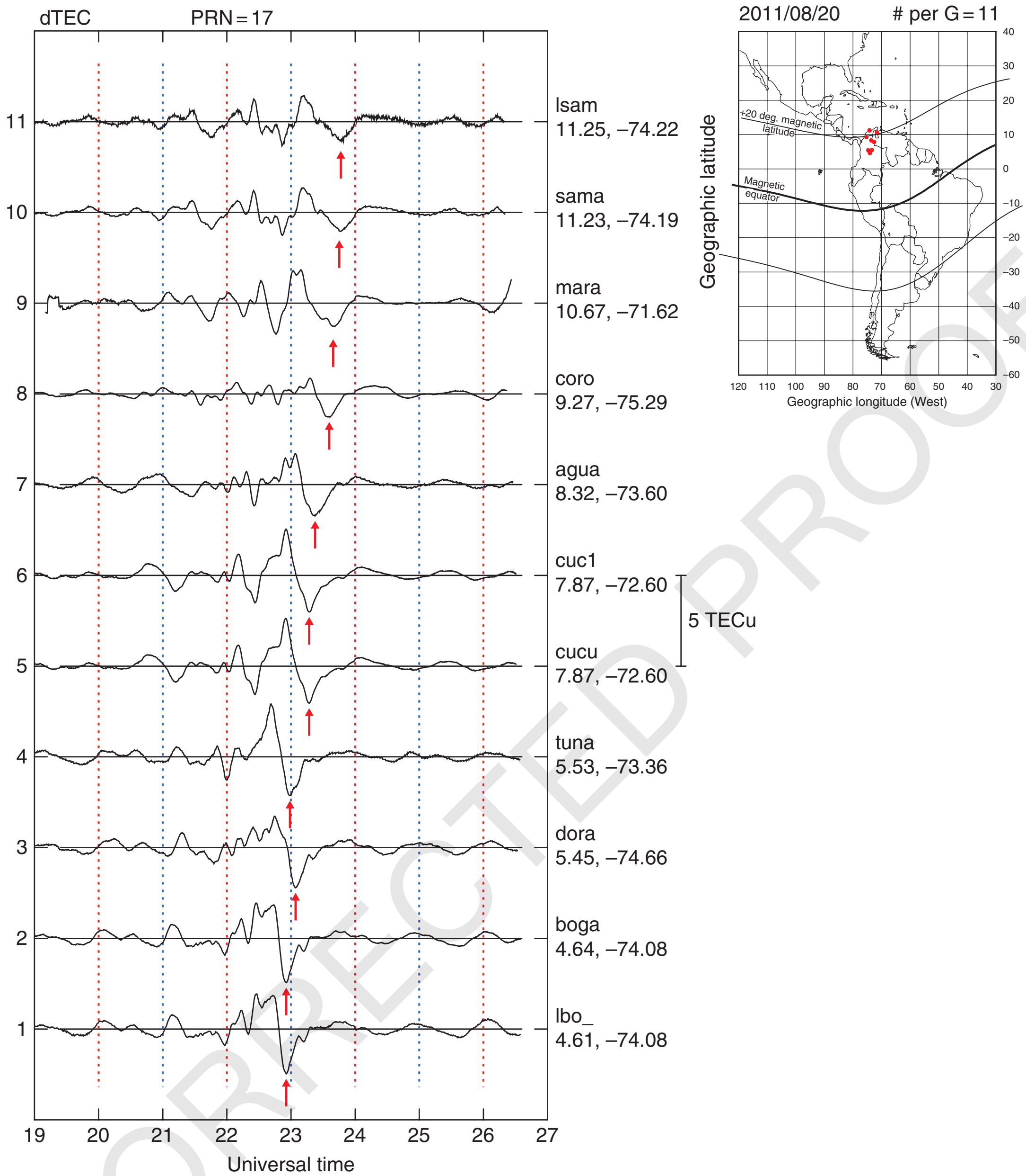

Figure 16.6 TEC perturbation (dTEC) values measured by 11 stations located in northern Colombia and Venezuela. The red arrows indicate the time when the minimum dTEC value was found in each trace. The four-letter GPS station code and the latitude and longitude for each station are printed on the right margin. The red dots in the upper-right frame indicate the geographic location of the 11 stations.

ward at 24 UT. These values confirm the direction of motion that was determined based on the time shift of the largest minimum of Figure 16.6. At the same time, they provide a more precise estimate of the TID transit motion. It is indicated that similar phase velocities were determined when our analysis procedure was performed using other receivers that belong to the GPS cluster of Figure 16.6.

16.3.3. Regional Maps of TIDs Velocity for 20–21 August 2011

Figure 16.8 compiles the TIDs' velocity information from the majority of the GPS clusters. Red vectors indicate northward velocities and blue vectors depict velocities with a southward component. The velocity field was decimated a factor of 8 to avoid cluttering the figure. The

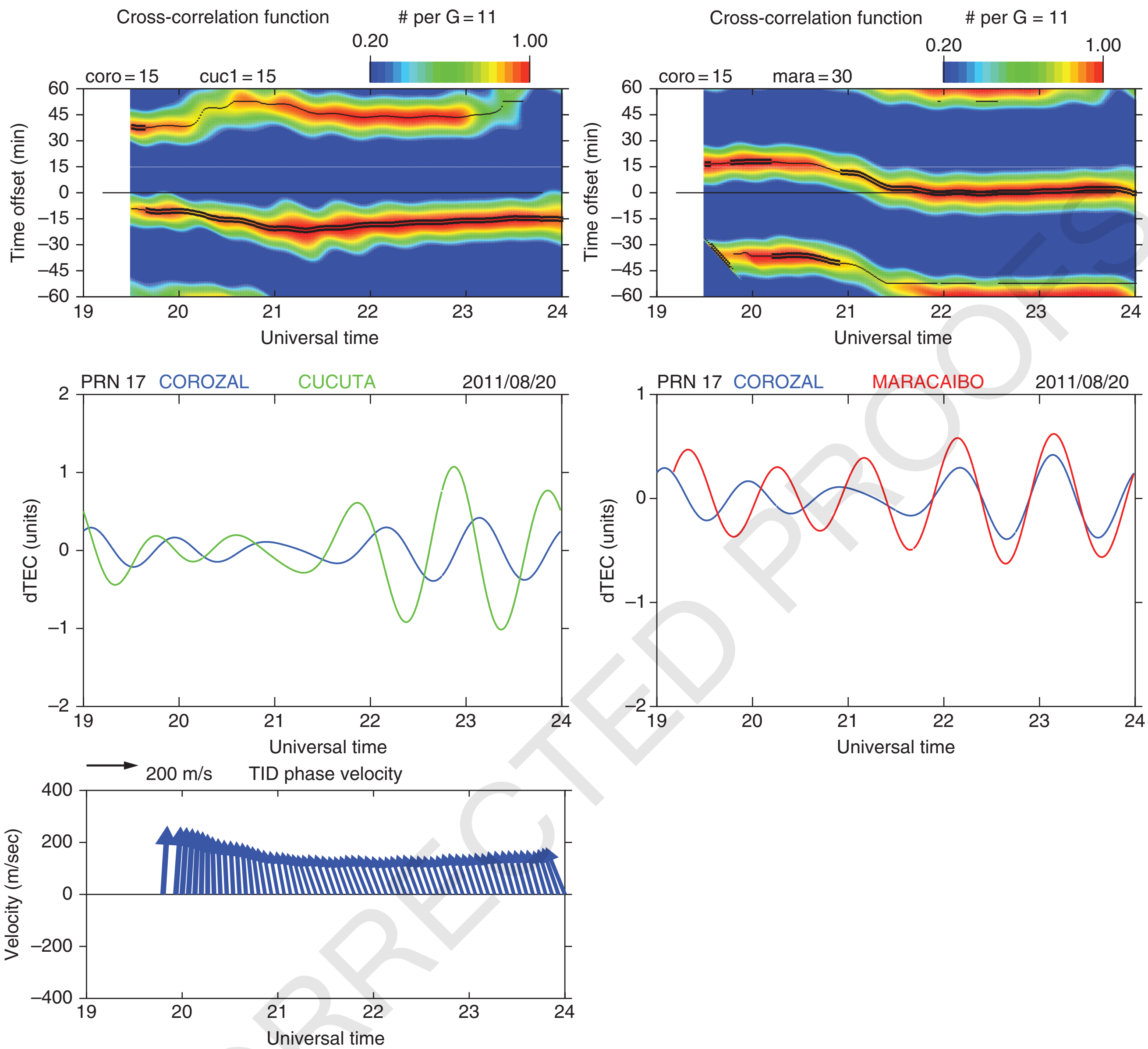

Figure 16.7 Same as Figure 16.3, but for GPS satellite 17 and stations Corozal and Cucuta in the left frames and Corozal and Maracaibo in the right frames. The unfiltered dTEC values for these three stations are displayed in Figure 16.6. The lower panel shows the phase velocities of the TIDs calculated using the time delays provided by the CCM algorithm (upper frames).

main characteristic of the plots is the general trend of the velocities: they are principally directed northward or southward. However, there exist some exceptions and the TID velocity can have a small westward or eastward component during the early evening and early hours of the day. On 20 August 2011 at 16 UT, the velocities over South America vary between 200 and 500 m/s. At this time, the TIDs' velocities are mainly directed northward with a ±20° directional variability. The following frame corresponding to 20–24 UT shows the velocities directed northwestward in the northern part of South America. These velocities intrude into Central America reaching values as high as 400 m/s. There also exists a region near Puerto Rico where velocities are directed southeastward reaching 420 m/s.

The next frame, corresponding to 21 August 2011 at 00–04 UT, displays velocities over the eastern side of the Caribbean region, where the flow is ~200 m/s, and it is directed southwestward. Downstream in eastern Colombia, the TIDs' velocities were also pointing southwestward, but the velocity magnitude was ~300 m/s. On the same day and between 12 and 16 UT, TID activity

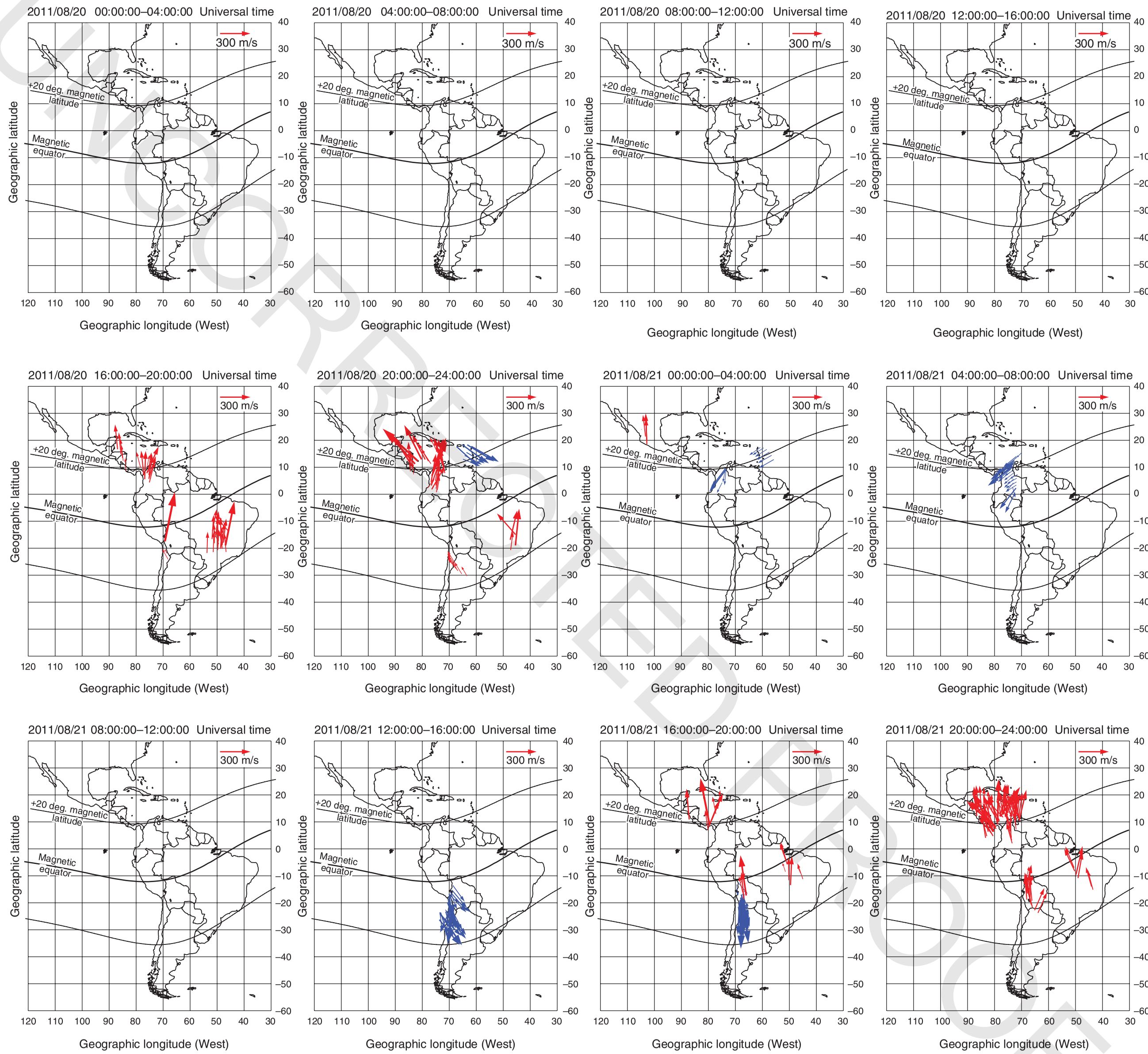

Figure 16.8 TIDs' phase velocities calculated using the CCM algorithm. See text for further details of the method employed to calculate the velocities. Red arrows are used for velocities having a northward component. Blue arrows correspond to velocities that have a southward component.

develops near the border between Peru, Bolivia, and Chile with velocities in the range of 300–400 m/s. Between 16 and 20 UT, there exists a region over central Bolivia where counter-streaming TIDs' velocities are found. We interpret this event as the superposition of two different trains of TIDs that are transiting in opposite directions, but propagating across two very close or overlapping volumes. The last frame indicates that the flow of TIDs is mainly northward over two regions separated by thousands of kilometers. One is located in the central part of South America and the other in Central America.

16.3.4. GOES-12 Infrared Images

The Geostationary Satellite system (GOES) mission provides weather monitoring, and aids research to understand land, atmosphere, ocean, and climate interactions. GOES-12 was launched in 2001, and has been in standby orbit most of its lifetime. However, during a few months in 2011, GOES-12 operated in the GOES-EAST position (parked in geostationary orbit at 60°W), providing coverage of the east coast of the United States and South America. The spacecraft was designed to "stare" at the Earth and image clouds, monitor Earth's surface temperature and water vapor fields, and sound the atmosphere for its vertical thermal and vapor structures. Therefore, the evolution of atmospheric phenomena can be followed, ensuring real-time coverage of short-lived dynamic events, especially severe local storms and tropical cyclones.

The imager on board GOES-12 is a multichannel instrument that senses infrared radiant energy and visible reflected solar energy from the Earth's surface and atmosphere. The satellite also measures the temperature of the clouds and the surface of the Earth with an infrared sensor. This allows for the detection of changes in the temperature of clouds during the day and at night. The temperature of the clouds also indicates how tall clouds are since temperature is usually inversely proportional to height in the troposphere. Red color indicates the appearance of temperatures as cold as −80°C and clouds extending up to 11,000–12,000 m. *Vadas and Crowley* [2010] pointed out that the type of clouds that prevail in Central and South America consist of convective plumes able to trigger gravity waves that propagate through the troposphere and mesosphere, which dissipate in the thermosphere (or mesosphere) and create body forces that are able to generate secondary gravity waves that can reach F-region altitudes.

Figure 16.9 shows four images taken with the infrared sensor on board GOES-12 between (1) 20 August 2011 at 11:45 UT, (2) 20 August 2011 at 20:45 UT, (3) 21 August 2011 at 05:45 UT, and (4) 21 August 2011 at 17:45 UT. Images with a 3 hr cadence time can be found at the GOES website. Several series of convective plumes were seen within Central and South America during two days when tropical storm Irene developed in the Caribbean region (see storm indicated with a yellow arrow in Fig. 16.9a). The first frame, corresponding to 11:45 UT on 20 August 2011, shows the remnants of a tropical depression that originated over the Pacific Ocean, drifted northeast, and was located over Central America at the time of the GOES-12 image. Figure 16.9a also displays the formation of a tropical depression moving north of the northern coast of South America (yellow arrow). A few hours later this tropical depression became organized enough to be classified as tropical storm Irene.

Figure 16.9b shows Irene transiting through the Caribbean region before it became a category 1 hurricane. This frame displays a cluster of convective plumes that extended through the southern part of Peru and western Brazil (see yellow ellipse). This frame also provides evidence for the presence of another region of very cold temperatures located to the east of the southern tip of South America and close to Antarctica. This region persists for many hours until 14:45 UT on 21 August 2011. Figure 16.9c shows the northward expansion of this region of cold temperatures seen close to Antarctica (enclosed by a yellow ellipse). Figure 16.9d shows the continuing energization of Hurricane Irene that displays a cluster of convective cells with temperatures below −80 °C. Figure 16.9d indicates the decay of the majority of convective cells seen in previous frames. This frame also displays the initiation of a new cluster of convective plumes near northern Peru and extending into Brazil in the western side of South America (yellow line).

16.4. PROPAGATION ANALYSIS OF THE TIDS MOVING ACROSS CENTRAL AND SOUTH AMERICA

This section presents an origin finding analysis aiming to associate the characteristics of the TIDs observed by several networks of GPS receivers in South and Central America, with corresponding regional images of tropical storms and tropospheric convective cells detected by the GOES-12 satellite. The cause-effect relationship is investigated using recent results from several experimental and modeling studies of AGWs conducted by *Fritts and Vadas* [2008], *Vadas and Liu*, [2009], and *Vadas and Crowley*, [2010]. It is known that atmospheric gravity waves (AGW) can be initiated at polar regions due to extreme Joule heating that is deposited during magnetic storms [*Saito et al.*, 1998; *Shiokawa et al.*, 2002; *Valladares et al.*, 2009]. Similarly, AGWs can also be triggered by earthquakes [*Galvan et al.*, 2011], tsunamis [*Makela at al.* 2011], nuclear explosions, tropospheric deep convective cells [*Hocke and Tsuda*, 2001; *Bishop et al.* 2006], and thermosphere body forces [*Fritts and Luo*, 1992; *Vadas and Fritts*, 2001]. This study introduces observations of 20 and 21 August 2011 in which neither earthquakes nor

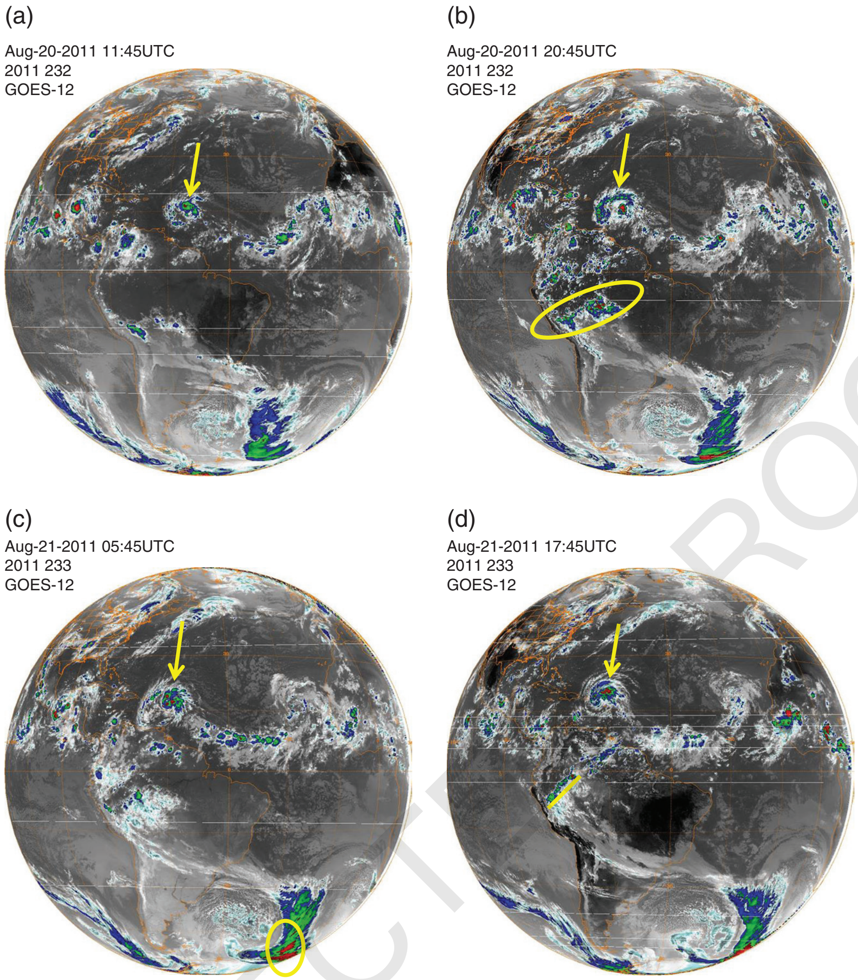

Figure 16.9 Four images observed with the GOES 12 satellite corresponding to (a) 20 August 2011, 12:00 UT; (b) 20 August 2011, 21:00 UT; (c) 21 August 2011, 06:00 UT; and (d) 21 August 2011, 18:00 UT. Yellow symbols indicate important features in the images such as a tropical storm Irene (arrows) and deep convective cells (ellipses).

tsunamis nor nuclear explosions occurred. In addition, during these 2 days magnetic activity was quiet. We discuss below the association of TIDs observed on 20–21 August 2011 in the American sector, and primary and secondary AGWs triggered by the tropical storm Irene that developed in the Caribbean region, and/or deep convective plumes that developed over or near South America.

When primary AGWs are created near the tropopause, they travel outward from the origin in all directions forming at mesospheric altitudes an almost circular pattern of perturbed densities. At higher altitudes, the variable thermospheric wind filters the AGWs in some directions leaving a segmented pattern of AGWs propagating only at selected directions. Saturation, wind filtering, and wave breaking make the primary waves dissipate and transfer momentum to the atmosphere creating horizontal body forces [*Vadas and Fritts*, 2004]. AGWs containing large-scale sizes might be able to propagate to the F-region bottomside. Smaller-scale AGWs (20–30 km) dissipate at 90 km and others with larger sizes (50–150 km) at 140 km, creating mesospheric and thermospheric body forces, respectively [*Vadas and Crowley*, 2010]. These body forces excite large-scale, upward and downward propagating secondary AGWs and then TIDs with scale sizes between 1000 and 2000 km, horizontal velocity ~500 m/s, and periods ~80 min, which propagate away from the body forces, traveling up to altitudes as high as 400 km [*Vadas and Liu*, 2009]. AGWs propagating against the neutral wind can reach the F-region bottomside and produce TIDs by moving plasma along the magnetic field lines [*Hines and Reddy*, 1967; *Fritts and Vadas*, 2008]. However, AGWs propagating in the same direction of the neutral wind dissipate due to the wind-filtering effect.

We have used GPS receivers (279) belonging to several networks that operated across the South American continent and the Caribbean region in 2011 to observe and characterize TIDs in these regions. If the velocity of the AGWs is constant, then their signatures will reach the different stations at different instants depending on the separation between the stations and the place of the AGWs' origin. Therefore, any feature of the TIDs (e.g., valleys, peaks) will align linearly in a travel distance versus universal time diagram. We have used this property of the TIDs to find their propagation velocity, and also to search for the locations where the body forces excited secondary waves and the places where deep convective plumes generated primary waves. Thus, this method can be used to define the inception point of the TIDs.

The four frames of Figure 16.10 show the TEC perturbations in a distance versus universal time format. These diagrams are similar to the travel time versus universal time plots presented by *Galvan et al.* [2012]. These authors calculated the travel velocity of Rayleigh, acoustic, and gravity waves associated with the Tohoku tsunami as these different waves were sequentially observed by GPS receivers located farther distant from the epicenter. Figure 16.10 shows the TEC perturbations corresponding to four events of TIDs associated with primary and secondary AGWs that developed on 20 and 21 August 2011. These diagrams display perturbation troughs and crests traveling at a constant velocity that are aligned with straight lines. Because we do not have a priori information about the geographic location where the thermospheric body forces excited secondary AGWs, we searched for the geographic latitude and longitude that made the troughs and crests align along parallel lines. This method provides

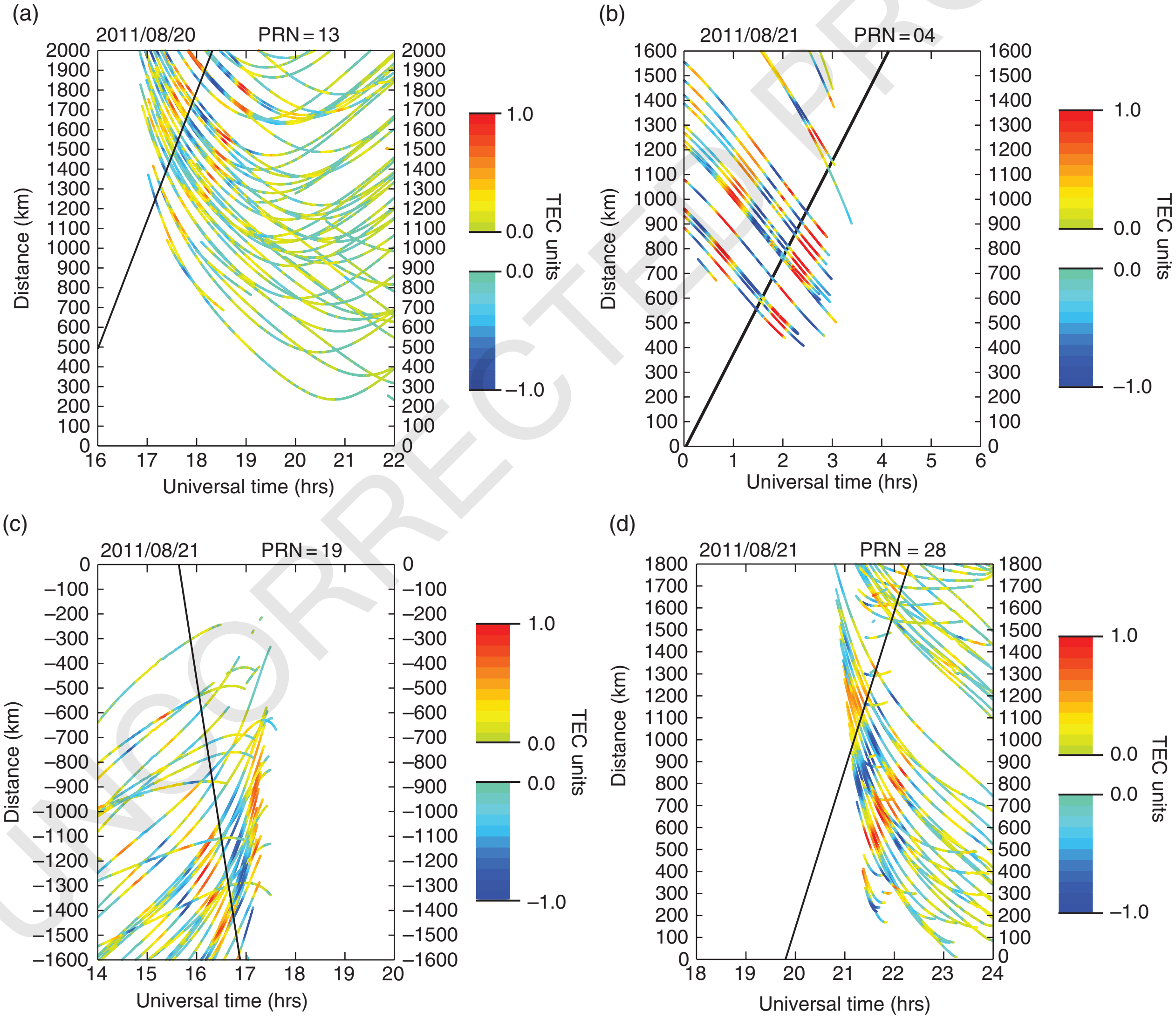

Figure 16.10 Travel time (distance) as a function of Universal Time plots corresponding to the following four events: (a) 20 August 2011, 16–22 UT. (b) 21 August 2011, 0–6 UT. (c) 21 August 2011, 14–20 UT. (d) 21 August 2011, 18–24 UT. Note that we have used negative distances in panel (c) as the TIDs were moving southward.

a good estimate of the geographic location of the body forces and/or the deep convective plumes.

Figure 16.10a displays the TEC perturbations from PRN 13 measured between 16 and 22 UT on 20 August 2011. These TEC perturbations were also displayed in Figure 16.5 (see number 1 in frame corresponding to 16–20 UT). They are observed south of the magnetic equator, over the eastern part of Brazil. We found that an origin placed at Lat = 34°S and Long = 50°W produced TECP peaks (red) and valleys (blue) forming parallel lines. This origin or center place is about 2° off the southern coast of Brazil and near the border with Uruguay. The slope of the line delineated in this figure gives a velocity equal to 208 m/s. However, a more precise calculation of the TID velocity, as shown in Figure 16.8, provided a value of 250 m/s. The peak-to-peak amplitude of the TEC perturbations presented in this frame and the following is close to ±1 TEC unit.

Figure 16.10b shows a trail of TEC perturbations from PRN 04 measured between 00 and 06 UT on 21 August 2011. During this event, the TIDs' velocity was equal to 135 m/s. This value is close to the TIDs' phase velocity calculated in Section 16.3.3 that indicated a velocity equal to 140 m/s directed westward. This velocity is in the range of primary AGWs that are able to propagate up to the F-region bottomside. The period and scale size of the TIDs of Figure 16.10b are about 30 min and 250 km, respectively. We also determined that the origin of the TIDs was at 18°N, 54°W. This location is within the broad extension of tropical storm Irene (see Fig. 16.9a), which was centered near 15°N and 59°W on 21 August 2011 at 00 UT. Images of the GOES-12 satellite indicated a region of low temperature (−80°) observed near 16°N, 54°W (see Fig. 16.9b) and within the reach of TS Irene. Figure 16.10b also indicates that the average distance between the TID observations and the point of origin varied between 400 and 1400 km. As some of the TIDs were observed 1400 km away, it is possible to infer that these waves were likely generated ~2.5 hr before 00 UT and, as stated before, within the vicinity of tropical storm Irene.

Figure 16.11 shows precipitation rainfall measured by the Tropical Rainfall Measuring Mission (TRMM) satellite on 21 August 2011 at 00 UT. TRMM is a joint

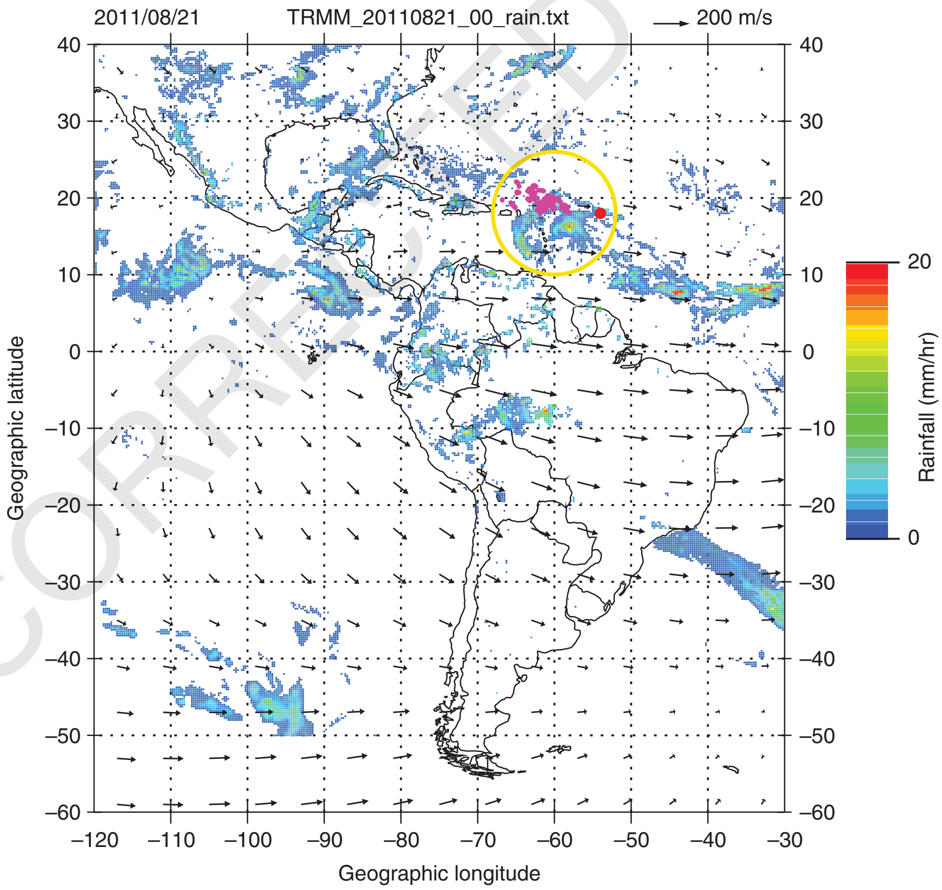

Figure 16.11 Rainfall measured by the TRMM satellite over South and Central America and the Caribbean region on 21 August 2011 at 00 UT. Note the region of heavy rain at the location of the tropical storm Irene. The large red dot indicates the location of the origin of the dTEC perturbations displayed in Figure 16.10b. The positive values of dTEC, displayed in Figure 16.10b, are displayed in purple.

US-Japan satellite mission to monitor tropical and subtropical precipitation and to estimate its associated latent heat. Figure 16.11 displays (1) the amount of rainfall in mm/hour in the American sector, (2) black arrows representing neutral wind vectors from the Hedin Wind model (HWM) at 200 km altitude [*Hedin et al.*, 1988], and (3) TEC perturbations (in purple). Note that the TECPs and the rain associated with TS Irene are contained inside a yellow circle. Figure 16.11 points out that the neutral wind velocity over the Caribbean region, where TS Irene developed, is ~100 m/s directed eastward. This magnitude and direction of the wind make waves propagating eastward dissipate. However, it favors the propagation of AGWs in the opposite direction as seen in Figure 16.8.

Figure 16.10c displays the signature of TIDs from PRN 19 measured on 21 August 2011 between 14 and 20 UT. Note that the axis of the travel distance is labeled using negative distances due to the southward propagation of the TIDs. The negative slope in this plot indicates TIDs moving southward from the origin located at 6°S, 72°W. The TID velocity is equal to 420 m/s, in agreement with the phase velocity displayed in Figure 16.8. The scale sizes and periods of the TIDs are equal to 1750 km and 65 min. We suggest that these TIDs are associated with secondary AGWs excited by body forces in the mesosphere or thermosphere. It is worth mentioning that Section 16.3.4 introduced a region of deep convective cells that developed over northern Peru and the western part of Brazil (see yellow line in Fig. 16.9d). This region was active between 12 and 21 UT on 21 August 2011 and decayed shortly after 21 UT.

Figure 16.10d depicts TEC perturbations from PRN 28 measured between 18 and 24 UT on 21 August 2011. The origin of these TIDs was found to be located at 22°S, 68°W. This location is in the northern part of Chile close to the border with Bolivia. The slope in the boundary between positive and negative TECP excursions indicates a velocity equal to 250 m/s and directed northward. The phase velocity of the TIDs was also calculated in Section 16.3.3 using the CCM delay method and equations (16.1) and (16.2) resulting in a value equal to 300 m/s. This large velocity and the fact that the scale size of the TID was of order 1000 km indicate an association with secondary AGWs and not with primary waves that usually have small scale sizes and velocities less than 180 m/s. Therefore, we suggest that the TIDs in Figure 16.10d were excited by mesosphere or thermosphere body forces centered at 22°S, 68°W. We have shown in Figure 16.8 that the TIDs were moving northward on 21 August 2011, between 20 and 24 UT. Based on these arguments, we conclude that these waves might have originated in the southern part of South America or probably farther south near Antarctica (see yellow ellipse in Fig. 16.9c for an extended region of red indicating low temperatures). This region near Antarctica seems a likely place to excite AGWs that could be propagating northward to the South American continent.

16.5. DISCUSSION

This chapter presents the results of an analysis program built to calculate the characteristics of TIDs propagating across South and Central America and the Caribbean region. This method uses TEC values measured by the LISN GPS receivers and several other networks of GPS receivers that are presently operating in these regions. This type of analysis can be extended to include other regions of the globe or applied to other low and/or midlatitude regions, such as the African, European, or Asian continents, to investigate the dynamics of TIDs in a larger regional or global context. In essence, the analysis provides regional maps of the population, the phase velocity, and the scale size of the TID waves. When this analysis is combined with theoretical and modeling results of the generation and propagation of AGWs, it is possible to derive information of the place of origin of the TIDs and the nature of AGWs responsible for the TIDs (e.g., primary versus secondary).

We found that on 20 and 21 August 2011, the TIDs' phase velocity was highly variable. We obtained phase velocities between 140 and 500 m/s. This velocity variability was too large to conclude that all TIDs corresponded to secondary waves excited only by thermospheric or mesospheric body forces. It is proposed that at least one event corresponded to primary AGWs produced by tropospheric convective overshoot that occurred in the proximity of tropical storm Irene. We also found that the TIDs, observed on these 2 days, contained scale sizes between 250 and 1800 kms, and periods between 30 and 70 min. Waves with smaller periods (20 min) were detected but not fully analyzed.

To find the locations where the TIDs originated, we searched for the geographic location that made crests and valleys of TECP to align along parallel lines in a distance versus time plot (Fig. 16.10). This method was based on the notion that AGWs propagate as concentric rings away from a central focal point. This center point could be the geographic location of a cluster of convective cells in the tropopause (for the generation of primary AGWs) or the region of body forces on the thermosphere-mesosphere system (for the generation of secondary AGWs). Our principal objective was to investigate the possibility if any of these origins coincided with regions of tropospheric deep convective plumes that were detected by the GOES-12 satellite (Fig. 16.9). We suggest that one out of the four cases analyzed in this publication is likely associated with primary AGWs triggered within TS Irene.

Figure 16.10a introduced a cluster of TIDs observed between 16 and 22 UT over Brazil that were propagating northward with velocities between 200 and 300 m/s. These TIDs are displayed in Figure 16.5 and indicated with a number 1. Figure 16.10d introduced another cluster of TIDs located at the same geographic latitude as the TIDs in Figure 16.10a. They contained similar velocities and occurred at similar universal times. These TIDs are indicated with a number 4 in Figure 16.5. Due to their similarity, we suggest that these two sets of TIDs were produced by thermospheric body forces responding to almost similar inputs that operate on a daily basis. The common source could be a region of cold temperatures near Antarctica (yellow circle in Fig. 16.9c) or very high wave/tide activity near the southern tip of South America. The latter region is considered a steady source of tropospheric and mesospheric waves (D. Janches, personal communication). This source of AGWs was probably active almost every day between 16 and 24 UT, for the following 10 days. More analysis is needed to determine the seasonal and day-to-day variability of the TIDs in this region.

Figure 16.10b (number 2 in Fig. 16.5) seems to be closely related to the presence of TS Irene. However, TIDs are only observed between 20 and 08 UT on the following day. This temporal constraint is likely due to the wind-filtering effect that dissipates waves when their velocity becomes almost parallel with the neutral wind motion. Figure 16.11 indicates that at 00 UT on 21 August 2011, the wind is directed eastward favoring the propagation of westward-directed AGWs. Figure 16.10c (number 3 in Fig. 16.5) and Figure 16.8 displayed the existence of a channel of TIDs propagating southward in the opposite direction to the majority of TIDs that prevailed after 17 UT on 21 August 2011. Based on the magnitude and direction of the phase velocity, the scale size, and period of the TIDs, it is suggested that these southward propagating TIDs were excited by thermospheric sources produced by the dissipation of primary AGWs that originated within TS Irene or in the region of several convective plumes that occurred in the northern part of Peru (see yellow line in Fig. 16.9d).

On 20 and 21 August 2011, TIDs in the America sector propagated mainly in the geographic northward and southward directions. TIDs velocities larger than 300 m/s directed northward were observed across South America. These velocities seem to correspond to secondary AGWs that were probably generated thousands of kilometers away, and quite likely between the continent and Antarctica. However, an important deviation from the strictly north-south velocity existed. Near TS Irene, westward velocities were observed between 01 and 03 UT on 21 August 2011. Eastward velocities were also seen near TS Irene a few hours prior to the event presented in Figure 16.10b. As the TIDs were detected very close to TS Irene, it was suggested that they may correspond to primary AGWs excited by tropospheric sources. We also found a region of counter-streaming TIDs separated by less than 100 km.

The regional plots presented in Figures 16.5 and 16.8 show the variability of the TID activity during 2 days: 20 and 21 August 2011. These 2 days are magnetically quiet periods and point out an absence of large-scale TIDs (>2000 km) that are commonly observed during large magnetic storms. It has been reported by *Valladares et al.* [2009] that during times of magnetic activity, large-scale TIDs move toward the equator from the poles. However, the TIDs reported here were likely generated in the midlatitude or low-latitude troposphere, mesosphere, or thermosphere.

16.6. CONCLUSIONS

This study has led to the following:

1. This analysis has provided regional maps of TEC perturbations associated with the TIDs that circulated throughout South and Central America and the Caribbean region on 20 and 21 August 2011. Similar plots can be constructed for other continents such as Africa and Asia to further our understanding on the longitudinal differences that exist in different regions of the globe.
2. Calculations of the phase velocity and the scale size of TIDs and regional images of tropospheric temperature brightness recorded by the GOES-12 satellite were used to assess the role of a tropical storm and clusters of tropospheric convective cells on the initiation of TIDs in the South American continent.
3. A group of TIDs, observed in the Caribbean region between 0 and 06 UT on 21 August 2011, were likely associated with primary AGWs. These waves were triggered within the region of TS Irene. These TIDs were moving eastward at 140 m/s and had a scales size of 250 km.
4. TIDs associated with primary and secondary AGWs were identified and an estimation of their place and time of origin was calculated using plots of the TEC perturbations in a travel-distance versus universal time format.

ACKNOWLEDGMENTS

The authors thank Dr. Claudio Brunini and Mauricio Gende of the Geocentric Reference System for the Americas (SIRGAS) and Dr. Michael Bevis from Ohio State University - Central and Southern Andes GPS Project (OSU-CAP) for providing GPS data. Dr. Hector Mora from the Colombian Institute of Geology and Mining (INGEOMINAS) provided RINEX files from several stations in Colombia. One of the authors, Dr. Valladares, was partially supported by Air Force Research Laboratory contract FA8718-09-C-0041, NSF Grants ATM-1135675, and ATM-1242476 and NASA LWS Grant NNX11AP02G. The Low-Latitude Ionospheric Sensor Network (LISN) is a project led by Boston College in collaboration with the Geophysical Institute of Peru, and other institutions that provide information in benefit of the scientific community. We thank all organizations and persons that are supporting and operating receivers in LISN. The TEC values presented in this publication are stored in the LISN web page (http://lisn.igp.gob.pe).

REFERENCES

Afraimovich, E. L., et al. (1998), GPS radio interferometry of travelling ionospheric disturbances, *J. Atmos. Sol. Terr. Phys.*, *60*, 1205–1223.

Afraimovich, E. L., et al. (2000), Determining parameters of large-scale traveling ionospheric disturbances of auroral origin using GPS-arrays, *J. Atmos. Sol. Terr. Phys.*, *62*, 553–565.

Afraimovich, E. L., E. A. Kosogorov, N. P. Perevalova, and A. V. Plotnikov (2001), The use of GPS arrays in detecting shock-acoustic waves generated during rocket launchings, *J. Atmos. Sol. Terr. Phys.*, *63*(18), 1941–1957.

Afraimovich, E. L., N. P. Perevalova, and S. V. Voyeikov (2003), Traveling wave packets of total electron content disturbances as deduced from global GPS network data, *J. Atmos. Sol. Terr. Phys.*, *65*(11–13), 1245–1262.

Bishop, R., N. Aponte, G. D. Earle, M. Sulzer, M. Larsen, and G. Peng (2006), Arecibo observations of ionospheric perturbations associated with the passage of tropical storm Odette, *J. Geophys. Res.*, *111* (A11), A11320; doi:10.1029/2006JA011668.

Crowley, G., and F. S. Rodrigues (2012), Characteristics of traveling ionospheric disturbances observed by the TIDDBIT sounder, *Radio Sci.*, *47*, RS0L22; doi:10.1029/2011RS004959.

Fritts, D. C., and S. L. Vadas (2008), Gravity wave penetration in to the thermosphere: Sensitivity to solar cycle variations and mean winds, *Ann. Geophys.*, *26*, 3841–3861.

Fritts, D. C., and Z. Luo (1992), Gravity wave excitation by geostrophic adjustment of the jet stream, Part1: Two-dimensional forcing, *J. Atmos. Sci.*, *49*, 681–697.

Galvan, D. A., A. Komjathy, M. P. Hickey, and A. J. Mannucci (2011), The 2009 Samoa and 2010 Chile tsunamis as observed in the ionosphere using GPS total electron content, *J. Geophys. Res.*, *116*, A06318; doi:10.1029/2010JA016204.

Galvan, D. A., A. Komjathy, M. P. Hickey, P. Stephens, J. Snively, Y. Tony Song, M. D. Butala, and A. J. Mannucci (2012), Ionospheric signatures of Tohoku-Oki tsunami of March 11, 2011: Model comparisons near the epicenter, *Radio Sci.*, *47*, RS4003; doi:10.1029/2012RS005023.

Hedin, A. E., N. W. Spencer, and T. L. Killeen (1988), Empirical global model of upper thermosphere winds based on Atmosphere and Dynamics Explorer satellite data, *J. Geophys. Res.*, *93*(A9), 9959–9978; doi:10.1029/JA093iA09p09959.

Hines, C. O. (1960), Internal atmospheric gravity waves at ionospheric heights, *Can. J. Phys.*, *38*, 1441–1481.

Hines, C. O., and C. A. Reddy (1967), On the propagation of atmospheric gravity waves through regions of wind shear, *J. Geophys. Res.*, *72*, 1015–1034.

Hocke, K., and K. Schlegel (1996), A review of atmospheric gravity waves and travelling ionospheric disturbances: 1982–1995, *Ann. Geophys.*, *14*, 917.

Hocke, K., and T. Tsuda (2001), Gravity waves and ionospheric irregularities over tropical convection zones observed by GPS/MET radio occultation, *Geophys. Res. Lett.*, *28*, 2815–2818.

Jacobson, A. R., and W. C. Erickson (1992), A method for characterizing transient ionospheric disturbances using a large radiotelescope array, *Astron. Astrophys.*, *257*, 401–409.

Jacobson, A. R., R. C. Carlos, R. S. Massey, and G. Wu (1995), Observations of traveling ionospheric disturbances with a satellite-beacon radio interferometer: Seasonal and local time behavior, *J. Geophys. Res.*, *100*(A2), 1653–1665; doi:10.1029/94JA02663.

Kirkland M. W., and A. R. Jacobson (1998), Drift-parallax determination of the altitude of traveling ionospheric disturbances observed with the Los Alamos radio-beacon interferometer, *Radio Sci.*, *33*(6), 1807–1825.

Makela, J. J., et al. (2011), Imaging and modeling the ionospheric airglow response over Hawaii to the tsunami generated by the Tohoku earthquake of 11 March 2011, *Geophys. Res. Lett.*, *38*, L00G02; doi:10.1029/2011GL047860.

Martinis, C., J. Baumgardner, J. Wroten, and M. Mendillo (2011), All-sky imaging observations of conjugate medium-scale traveling ionospheric disturbances in the American sector, *J. Geophys. Res.*, *116*, A05326; doi:10.1029/2010JA016264.

Mercier, C. (1986) Observations of atmospheric gravity waves by radio- interferometry, *J. Atmos. Terr. Phys.*, *48*, 605–624.

Otsuka, Y., K. Shiokawa, T. Ogawa, and P. Wilkinson (2004), Geomagnetic conjugate observations of medium-scale traveling ionospheric disturbances at midlatitude using all-sky airglow imagers, *Geophys. Res. Lett.*, *31*, L15803; doi:10.1029/2004GL020262.

Perkins, F. (1973), Spread *F* and ionospheric currents, *J. Geophys. Res.*, *78*(1), 218–226; doi:10.1029/JA078i001p00218.

Saito, A., T. Iyemori, and M. Takeda (1998), Evolutionary process of 10 kilometer scale irregularities in the nighttime midlatitude ionosphere, *J. Geophys. Res.*, *103*(A3), 3993–4000.

Shiokawa, K., et al. (2005), Geomagnetic conjugate observation of nighttime medium-scale and large-scale traveling ionospheric disturbances: FRONT3 campaign, *J. Geophys. Res.*, *110*, A05303; doi:10.1029/2004JA010845.

Shiokawa, K., Y. Otsuka, T. Ogawa, N. Balan, K. Igarashi, A. J. Ridley, D. J. Knipp, A. Saito, and K. Yumoto (2002), A large-scale traveling ionospheric disturbance during the magnetic storm of 15 September 1999, *J. Geophys. Res.*, *107*, 1088; doi:10.1029/2001JA000245.

Vadas, S. L. (2007), Horizontal and vertical propagation and dissipation of gravity waves in the thermosphere from lower atmospheric and thermospheric sources, *J. Geophys. Res.*, *112*, A06305; doi:10.1029/2006JA011845.

Vadas, S. L., and D. C. Fritts (2001), Gravity wave radiation and mean responses to local body forces in the atmosphere, *J. Atmos. Sci.*, *58*, 2249–2279.

Vadas, S. L., and D. C. Fritts (2004), Thermospheric responses to gravity waves arising from mesoscale convective complexes, *J. Atmos. Sol. Terr. Phys.*, *66*, 781–804.

Vadas, S. L., and G. Crowley (2010), Sources of the traveling ionospheric disturbances observed by the ionospheric TIDDBIT sounder near Wallops Island on October 30, 2007, *J. Geophys. Res.*, *115*, A07324; doi:10.1029/2009JA015053.

Vadas, S. L., and H. Liu (2009), Generation of large-scale gravity waves and neutral winds in the thermosphere from the dissipation of convectively generated gravity waves, *J. Geophys. Res.*, *114*, A10310; doi:10.1029/2009JA014108.

Valladares, C. E., and J. L. Chau (2012), The Low-latitude Ionosphere Sensor Network (LISN) initial results, *Radio Sci.*; doi:10.1029/2011RS004978.

Valladares, C. E., and M. A. Hei (2012), Measurement of the characteristics of TIDs using small and regional networks of GPS receivers during the campaign of 17–30 July of 2008, *Int. J. Geophys.*, Article ID 548784; doi:10.1155/2012/548784.

Valladares C. E., J. Villalobos, M. A. Hei, R. Sheehan, S. Basu, E. MacKenzie, P. H. Doherty, and V. H. Rios (2009), Simultaneous Observation of traveling ionospheric disturbances in the northern and southern hemispheres, *Annales Geophys.*, *27*, 1501.